NANO LETTERS

pubs.acs.org/NanoLett Letter

Widely Varying Kondo and Magnetic Interactions in Molecule Gold Nanostructured Materials by Changing the Gold Nanoarchitecture

Monique Tie,[⊥] Sean Colford,[⊥] Marek Niewczas, Ryan Baumbach, and Al-Amin Dhirani*

Cite This: https://doi.org/10.1021/acs.nanolett.2c04918 Read Online

ACCESS | Metrics & More | Article Recommendations | Supporting Information

ABSTRACT: Delocalized−localized electron interactions are central to strongly correlated electron phenomena. Here, we study the Kondo effect, a prototypical strongly correlated phenomena, in a tunable fashion using gold nanostructures (nanoparticle, NP, and nanoshell, NS) + molecule cross-linkers (butanedithiol, BDT). NP films exhibit hallmark signatures of the Kondo effect, including (1) a log temperature resistance upturn as temperature decreases in a metallic regime, and (2) zero-bias conductance peaks (ZBCPs) that are well fit by a Frota function near a percolation insulator transition, previously used to model Kondo peaks observed using tunnel junctions. Remarkably, NP + NS films exhibit ZBCPs that persist to >220 K, i.e., >10-fold higher than that in NP films. Magnetic measurements reveal that moments in NP powders align, and in NS powders, they antialign at low temperatures. Based on these observations, we propose a mechanism in which varying such material nanobuilding blocks can modify electron−electron interactions to such a large degree.

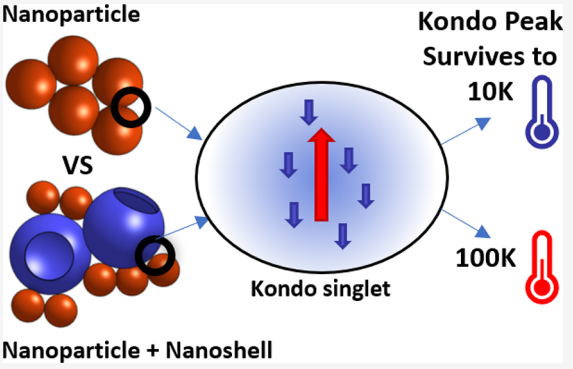

KEYWORDS: *gold nanoparticles, molecular self-assembly, nanostructured materials, antiferromagnetism, Kondo*

Interactions between unpaired localized electrons and conduction electrons are central to a number of important phenomena in condensed matter, including high T_c superconductivity and heavy fermion effects.[1−5] A test bed of such interactions is the Kondo effect in which antiferromagnetic coupling between unpaired localized electrons and conduction electrons leads to screening of the localized spins at sufficiently low temperature and the formation of a Kondo singlet state. This state gives rise to a Kondo resonance peak in density of states that is centered at the Fermi energy and increases in intensity significantly as temperature decreases below a characteristic Kondo temperature (T_K).

While the Kondo effect was originally observed in metal films with magnetic impurities,[6,7] the tunability of nanostructured materials has led to interest in studying the Kondo effect in these new systems.[8−13] Recent reports studied the Kondo effect exploiting the flexibility afforded by molecules, either on surfaces of metal films or in tunnel junctions. For example, one study has shown that it is possible to control coupling between gold electrodes and a molecule possessing a cobalt ion, polypyridine ligands, and a pair of alkanethiol chains, which tether the molecule to the gold: when using long alkane (i.e., pentane) dithiol tethers, single-electron charging is observed; however, when using short dithiol tethers (without an intervening alkane chain), the Kondo effect is observed due to strong coupling between the gold and the cobalt.[10] Spin dopant density can be controlled by self-assembling a monolayer composed of a mixture of transition metal complexes (either Co^{2+} or nonmagnetic Zn^{2+}) with terpyridine ligands tethered to the gold substrate via a single thiol end group. Changing the concentration of Co/Zn complexes enabled tuning the density of spin dopants up to record high values.[8] Using metal−organic interactions and the range of organic frameworks available, the range of choice for spin dopants can be extended. For example, Cu phthalocyanine molecules assembled onto a gold substrate exhibit a Kondo effect, while atomic Cu impurities themselves do not.[14] The Kondo effect has also been studied in larger, tunable architectures such as lithographically defined quantum dots (QDs).[15,16] Discrete electron charging effects are significant in QDs and can be varied as they depend on the size of the QD. In addition, by applying various gate voltages, energy levels within the QD can be shifted easily to generate unpaired/paired spin occupancy and effectively turn the Kondo effect on/off, respectively.

Assemblies of chemically synthesized nanoparticles provide a new target of opportunity to study the Kondo effect in a controllable platform. Previous studies have shown that

Received: December 17, 2022
Revised: April 25, 2023

https://doi.org/10.1021/acs.nanolett.2c04918
Nano Lett. XXXX, XXX, XXX−XXX

assemblies of Au nanoparticles (NPs) capped with alkanethiol molecules are magnetic, likely due to holes in gold d-orbitals at or near the NP surface.[17−21] Au−thiol bonding results in partial charge transfer from Au atoms to thiol, and X-ray measurements have shown an increase in density of 5d holes in Au when Au−thiol bonding was present.[18,19,22,23] This suggests a potential opportunity to study the Kondo effect using this system, in particular. This is an attractive system to explore the Kondo effect as Au NP + thiol/dithiol self-assembly has been widely studied.[24−27] Further, properties of this system can be tuned from the bottom-up through choice of nanostructured building blocks. Previous studies of magnetism in assemblies of Au NPs capped with alkanethiol molecules have focused on thiols with long alkane chains which render such assemblies insulating. Here, we study macroscopic conducting assemblies fashioned using short chain alkanedithiol (butanedithiol, BDT) linkers, Au NPs, and Au nanoshells (NSs). As in previous studies, localized spin states may occur at Au nanostructure surfaces, and at the same time, short BDT linkers used in the present study facilitate electron delocalization, charge transport down to sufficiently low temperatures, and observation of the Kondo effect.[17−19,25,28] Furthermore, we vary assembly structure by fabricating films using (1) all Au NPs and (2) alternating layers of Au NPs/Au NSs. We observe signatures of the Kondo effect in both BDT-linked NP and BDT-linked NP+NS films, and remarkably, in NP+NS films, the Kondo effect can persist beyond 220 K—more than 10-fold higher than that in NP films. Thick NP films are metallic, and near the percolation insulator−metal transition, films exhibit charge transport consistent with the presence of significant Coulomb interactions and tunneling. Thick NP+NS films remain insulating and exhibit larger Coulomb barriers than NP films. BDT-NP powders exhibit increasing moments with decreasing temperature (paramagnetism); in contrast, BDT-NS powders exhibit decreasing moments with decreasing temperature (suggesting moment antialignment). Combined, these data enable us to propose a microscopic picture for the range of behaviors observed. Given the observed strong relationship between nanobuilding block structure and electron−electron interactions, these results demonstrate a potential for the present system to serve as a platform to fashion quantum materials with controlled or nanoengineered behavior.

Previous studies have shown that Au NP films cross-linked with BDT undergo a percolation insulator-to-metal transition with increasing immersion cycles.[24] At lower immersion cycles, linked NP clusters are small and electronically isolated from each other. As the number of immersion cycles increases, clusters grow, and beyond a percolation threshold (PT) where clusters span the sample, films become metallic. Figure 1 shows normalized conductance (g) vs temperature (T) for a thick NP film well beyond the PT. The data exhibit a conductance maximum at ∼70 K. The inset shows the same data plot as normalized resistance (R) vs log (T). Below the minimum, resistance increases logarithmically as temperature decreases. A resistance minimum and a logarithmic upturn at lower temperatures are hallmark behaviors of the Kondo effect.[6] In contrast, NS films remain insulating even up to 23 immersion cycles when NP films are well beyond the PT. Conductance of the most conducting NS film is measurable down to only 8 K.

Figure 2a shows g vs voltage (V) data for a NP film. The data exhibit zero-bias conductance peaks (ZBCPs, observed in 5 of 12 samples). The peaks persist until ∼18 K, with peak heights that decrease and widths that increase with T. For reference, the peak height for the NP film at 2.5 K is ∼0.9 mS or about $\sim 12G_0$, where $G_0 = 2e^2/h$ is the quantum of conductance. This suggests that multiple parallel current pathways contribute to the ZBCP. We used ionic liquid gating to try to shift the peaks but find they remain at 0 V, i.e., at the Fermi level, excluding an underlying single-electron charging phenomenon. ZBCPs have been previously observed using localized spins in tunnel junctions where the localized spins coupled to conduction electrons in tunnel junction electrodes. The peaks arise due to an enhanced density of states at the Fermi level associated with the Kondo resonance.[9−12,29] We believe tunneling plays a significant role in charge transport in the present system and attribute the observed ZBCP to the Kondo resonance. Additional support comes from fitting the data using the Frota function:

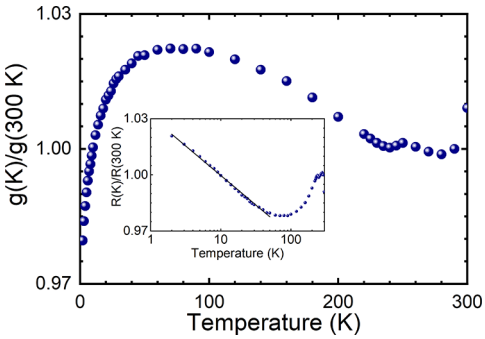

Figure 1. Normalized conductance (g) vs temperature (T) for a thick NP film well into the metallic regime. Inset: Normalized resistance (R) vs log (T) for the same film.

$$g(V) \propto \mathbb{R}\sqrt{\frac{i\Gamma_K}{i\Gamma_K + eV}} \tag{1}$$

where g is the measured conductance, V is the applied voltage, and Γ_K is the half-width at half-maximum (HWHM) of the ZBCP. Γ_K is related to the Kondo temperature via[30]

$$\Gamma_K = \sqrt{(\pi k_B T)^2 + (2k_B T_K)^2} \tag{2}$$

The Frota function has been previously shown to be effective in describing the Kondo resonance in other systems.[31] We find excellent agreement between the Frota function and our data over a wide range of temperatures (solid lines in Figure 2a). Further, in Figure 2c, we plot the HWHM obtained from the Frota fits vs T. Consistent with eq 2, as temperature decreases, widths decrease linearly and then plateau. As a further consistency test, g vs T data for this film exhibit a minimum which provides an estimate of $T_K \sim 6$ K or ∼0.5 meV (see Figure S3 in the Supporting Information);[32,33] and ZBCP widths in Figure 2a narrow to ∼0.25 meV at 2.5 K. Both temperature and voltage estimates for T_K are of the same order.

Figure 2b shows g vs V data for NP+NS films obtained on the insulating side of the PT which also can exhibit ZBCPs (observed in 3 of 25 samples). ZBCPs for NP+NS films can persist up to remarkably high temperatures exceeding 220 K, i.e., approximately an order of magnitude higher than those for NP films (∼18 K). At 100 K, the peak height is ∼0.01 μS or $\sim 1/8000G_0$. As before, peak widths increase linearly with T at these high temperatures, which agrees with the expected behavior of the Kondo resonance (see Figure 2d). Observed

https://doi.org/10.1021/acs.nanolett.2c04918
Nano Lett. XXXX, XXX, XXX−XXX

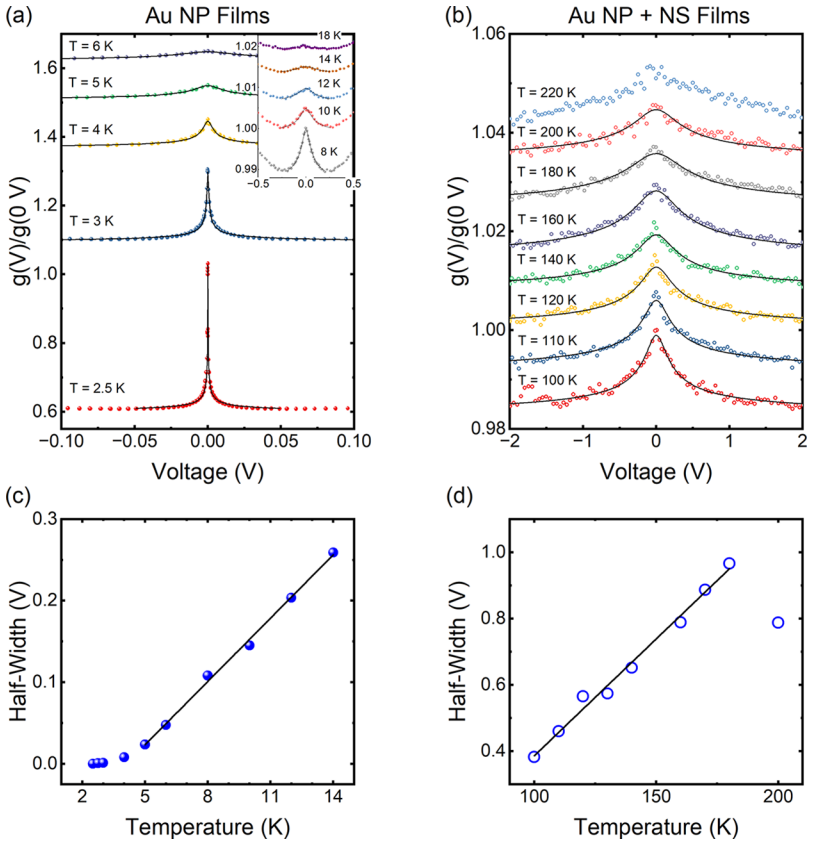

Figure 2. Transport data obtained using (a) NP and (b) NP+NS films: g vs V data taken at various temperatures, offset for clarity. Inset: Additional higher T data for NP films. Lines are fits using the Frota model. (c,d) Half-width of the peaks in (a,b) vs T. Absolute magnitudes of conductance measurements are given in Supporting Information Table S1.

peak half-widths at 100 K are ∼1V. Figure 2d and eq 2 show that widths increase linearly with T above T_K. As a result, these peak widths are thermally broadened. Also, these NP+NS films are insulating (see Figure S3 in the Supporting Information for g vs T data); such films likely contain many tunnel junctions in series which divide the applied voltage and further broaden the peak.

We can gauge the energy scale associated with T_K based on the temperature range over which ZBCPs survive. Figure 3 shows normalized ZBCP height data vs T obtained using 5 NP films and 3 NP+NS films. Typically, ZBCPs for NP films survive to ∼10 K, and for NP+NS films, they survive to >100 K.

Given our observation of various signatures of the Kondo effect in films, we used SQUID magnetometry to gain insight into the local moments driving the Kondo effect in these materials. Magnetic signals measured using thin films on quartz substrates, such as those used for transport measurements, were too low relative to background signals measured using just the quartz substrates. To improve the signal-to-noise, we prepared macroscopic quantities of cross-linked NP (20 mg) and NS (10 mg) powders, both cross-linked with BDT, and performed magnetic measurements using polymer-based powder sample holders from Quantum Design.

We measured magnetic moment (M) vs applied field (H) measurements for NP and NS powders contained in polymer powder sample holders, as well as background measurements for sample holders alone. In all cases, a diamagnetic response dominates. Figure 4 shows residuals obtained by fitting a line through high field measurements, beyond the saturation field,

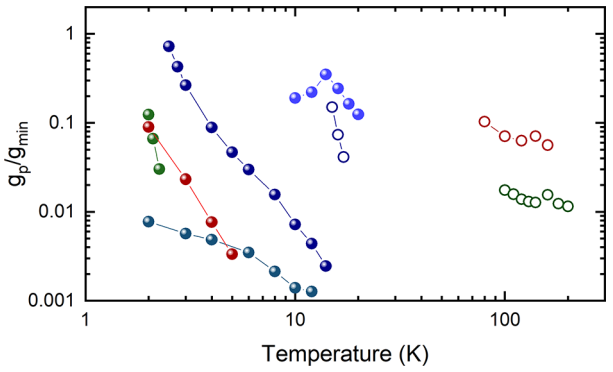

Figure 3. Value of log g_p/g_{min} (where g_p and g_{min} are ZBCP peak and minimum conductances, respectively, extracted from Frota fits) vs log T for 5 NP films (solid spheres) and 3 NP+NS films (hollow circles).

and subtracting this diamagnetic signal. See the Supporting Information for raw data as well as data for additional samples. NS powder and polymer sample holders exhibit a similar response, which we attribute to background caused by magnetic impurities that are off-centered with respect to the MPMS3's measurement coils. The NP powder exhibits a paramagnetic response that is ∼3× larger than this background with a slope of opposite sign. We estimate that the response for the NP powders corresponds to 3×10^{-4} emu/g or 4.9×10^{-2} μ_B/NP. Published values[20] range from 10^{-3} to 1 emu/g. These magnetic data suggest that the magnetic moments associated with the Kondo effect arise predominantly in BDT+NP structures.

https://doi.org/10.1021/acs.nanolett.2c04918
Nano Lett. XXXX, XXX, XXX−XXX

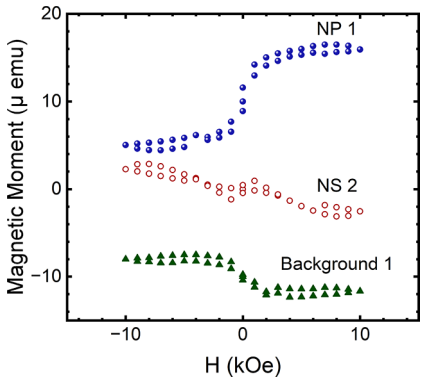

Figure 4. M (μ emu) vs H (kOe) after subtracting a diamagnetic background. Measurements taken at 2 K. The data are offset by 10 μ emu for clarity.

Figure 5a,b show M vs T data measured twice, both times applying a fixed 1 kOe field and increasing temperature: first after zero field cooling (ZFC) and then again after field cooling (FC) in a 1 kOe field. Below 70 K, all systems exhibit increasing moment with temperature, which we attribute to the sample holder (see the Supporting Information for measurements over the full temperature range). As temperature increases above 70 K, magnetic moments of NP and NS powders decrease and increase, respectively, while the moment of the background remains relatively constant.

To further analyze these behaviors, Figure 5c shows $1/M$ vs T obtained using two NP powder samples in both FC and ZFC conditions. The data are scaled with respect to M. We scale the data by fitting a line to the M^{-1} vs T data and using the calculated slope/intercept to scale each data set. For example, if the slope and intercept for this line are, respectively, A_x and B_x for sample X, then we scale the data as $(M_x^{-1} - B_x)/A_x$. Scaled data for any sample obeying Curie's law should collapse on this line. The scaled data exhibit a reasonably good linear trend below ∼200 K, which is consistent with Curie behavior and the paramagnetism exhibited by M vs H data for NP powders at 2 K. These results provide further evidence for the presence of magnetic moments in BDT-linked NP systems and support for the observation of the Kondo effect. Above 200 K, the paramagnetic signal from the NPs drops off, leaving only background signal. Data for different samples are scaled to overlap Curie contributions; however, background signals will not overlap, which leads to the observed divergence above 200 K.

Figure 5d shows corresponding M *vs* T data obtained for two NS powder samples. In contrast with data for BDT-linked NP powders which indicate moments paramagnetically align, FC and ZFC data for both NS powder samples split below a Neél temperature (T_N) of ∼120 K, indicating that moments in BDT-linked NS powders antialign at low temperatures and that a 1 kOe field is sufficient to overcome the antialignment (see Supporting Information for NS and background data comparing FC and ZFC measurements with averaging). At 2 K, M vs H data up to 10 kOe indicate that net moments in NS powders are smaller than those in NP samples. Assuming that the moment density for NPs provides an upper limit and assuming dipole−dipole interactions, we estimate that the temperature scale for dipole−dipole interactions[34] is multiple orders of magnitude below the Neél temperature of ∼120 K observed in NS powders. Given the large distances between moments, we can also exclude a superexchange mechanism.

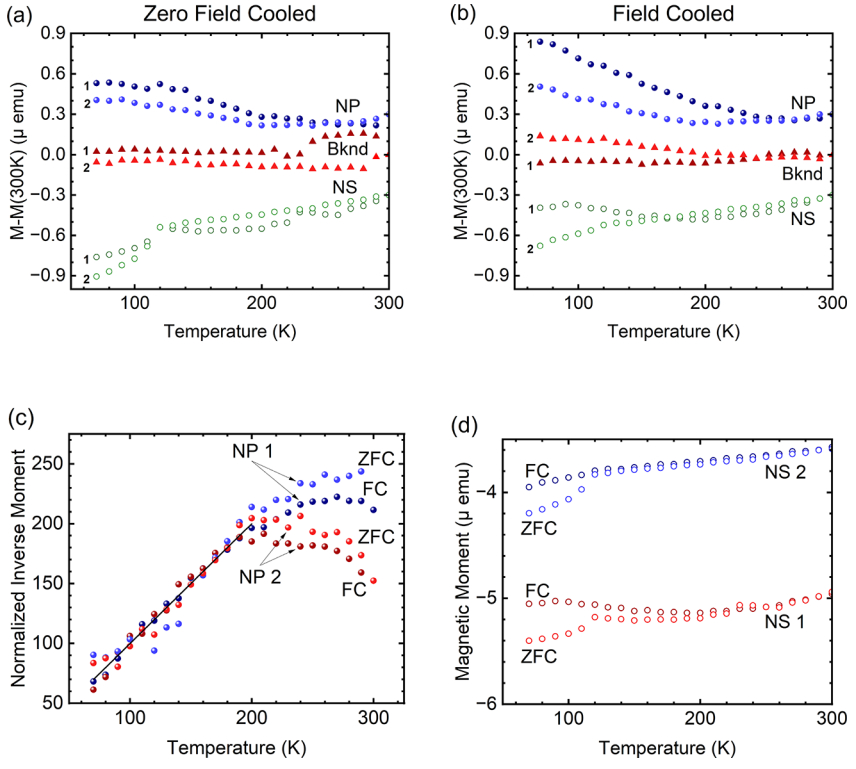

Figure 5. (a,b) M vs T. Data are offset by 0.3 μ emu for clarity. (c) Normalized inverse M vs T for two NP powder samples. Data are scaled such that the linear behavior overlaps. The straight line is shown to guide the eye. (d) M vs T for two NS powder samples in both ZFC and FC conditions.

https://doi.org/10.1021/acs.nanolett.2c04918
Nano Lett. XXXX, XXX, XXX−XXX

Accordingly, we propose that the Ruderman−Kittel−Kasuya−Yosida (RKKY) interaction mediated by conduction electrons as a plausible mechanism for the antialignment. The interaction energy, H_{RKKY}, between moments is given by[35]

$$H_{RKKY} = \frac{1}{2}\sum_{\mathbf{x},\mathbf{x}'} J_{RKKY}(\mathbf{x}-\mathbf{x}')\vec{\mathbf{S}}(\mathbf{x})\cdot\vec{\mathbf{S}}(\mathbf{x}') \quad (3)$$

where

$$J_{RKKY}(r) = J^2\rho\frac{1}{2\pi^2 r^3}\left[\cos 2k_F r - \frac{\sin 2k_F r}{2k_F r}\right] \quad (4)$$

$\vec{\mathbf{S}}$ is the spin of the local moment, J is a measure of the strength of the interaction, r is the distance between the local moments, ρ is the conduction electron density of states per spin, and k_F is the Fermi wavenumber. Although both NP and NS systems are chemically similar, their different magnetic behavior may arise from a difference in the hollow (insulating) NS vs solid (metal) NP nanostructure architecture. A transition to antiferromagnetic coupling can occur as free electron density and, correspondingly, k_F decreases at least locally. However, further studies are needed to detail the nature of the magnetic interactions in these materials.

While Au NPs comprise metal cores with delocalized electrons, NP surfaces are likely depleted of charge due to binding with electron-withdrawing thiols. Also, NP surfaces likely possess unpaired, localized d electrons associated with Au−thiol bonds, as previously reported in magnetic and X-ray studies of isolated alkanthiol-capped NPs.[36] Well beyond the PT, electrons can delocalize through sample spanning metallic clusters of BDT-linked NPs containing NP−NP interfaces; as a result, delocalized electrons can couple to unpaired d-electrons, generating signatures of the Kondo effect observed in the R vs T data (Figure 1). Closer to the PT, BDT-linked NP clusters are smaller, and films are more insulating. The importance of tunneling in overall transport in this regime is supported as tunneling conductance is proportional to density of states, and a ZBCP is observed, corresponding to the expected Kondo density of states peak at the Fermi level.

In the present study, we find that NP films exhibit Kondo peaks up to ∼20 K, while remarkably, NS+NP films exhibit peaks up to more than 10-fold higher temperatures exceeding 220 K. From plots of ZBCP widths vs T exhibiting saturation of widths at low temperature, we estimate $T_K \sim 4$ K for NP films. We cannot estimate T_K for NS films as at low temperatures film resistance becomes too high to measure, and the ZBCP width varies linearly over the accessible range of temperatures. However, since the temperature to which the Kondo peak survives increases with T_K, we infer that the T_K of NP+NS films are correspondingly higher. Previous studies using QD and single-molecule systems have reported T_K typically in a ∼10−30 K range.[9−13]

The Kondo temperature scale is given by[35]

$$T_K \sim \exp(-1/J\rho) \quad (5)$$

and since the Kondo effect persists to higher temperatures in NP+NS films than in NP films, $J\rho$ must increase. A number of observations indicate that ρ decreases in NP+NS films at least locally. g (proportional to density of states in tunneling) for NP+NS films is lower than that for NP films; also, NP+NS films remain insulating even after many immersion cycles, while NP films become metallic. That is, including insulating NSs results in isolation of conduction electrons. In order for T_K to increase in NP+NS films despite a decrease in ρ, J must correspondingly increase. Previous studies of Coulomb blockade using quantum dots have shown that charges can produce local fields which can shift quantum dot energy levels relative to the Fermi level.[37] Also, studies of heavy fermion materials have reported that increased hybridization of localized and delocalized states are associated with increased J.[38] In the present system, NSs are stabilized in water by sodium citrate charges on their surface which may be retained in the NP+NS films, potentially altering local moment and Fermi level energy alignment and increasing hybridization for some local moments.

Given a RKKY interaction between local magnetic moments and a Kondo interaction between local moments and conduction electrons, a Doniach phase diagram can be expected and may account for some of our observations: since T_K varies exponentially with J and ρ while T_N varies as a power law, Kondo moment screening should give way to RKKY-driven spin−spin interactions as J and ρ decrease. Our results suggest that starting from NP, adding NS causes J to increase and ρ to decrease (via lower NP concentration) such that $J\rho$ and T_K overall increase. However, pure NS systems have still lower ρ (since they are more insulating), and any potential increase in J does not compensate, so that $J\rho$ decreases overall. As a result, T_K drops below T_N, and NS powders exhibit magnetism as observed. Notably, ρ remains finite in NS films. Observation of surface plasmon resonance in NS films (Figure S1b(vi) in the Supporting Information) indicates the presence of delocalized electrons, at least locally, which could mediate the proposed RKKY interaction. Such an interplay between delocalized electrons and localized, unpaired electrons has been widely discussed in a context of Kondo lattices and transition metal/rare earth materials. Given that a variety of nanostructures and molecular cross-linkers are described in the literature, the present results point to a potential opportunity to use nanostructured materials as a tunable test bed to study such quantum strongly correlated electron−electron interactions, including up to rather high temperatures.

■ ASSOCIATED CONTENT

Supporting Information

The Supporting Information is available free of charge at https://pubs.acs.org/doi/10.1021/acs.nanolett.2c04918.

Additional experimental details, materials, nanostructure syntheses, nanostructured film/powder fabrication, and methods, MPMS-3 and PPMS-9 procedures, and complete magnetic data of all nanostructured powders, and absolute transport data of presented nanostructured films (PDF)

■ AUTHOR INFORMATION

Corresponding Author

Al-Amin Dhirani − *Department of Chemistry and Department of Physics, University of Toronto, Toronto, Ontario M5S 3H6, Canada;* orcid.org/0000-0003-3257-4327; Email: a.dhirani@utoronto.ca

Authors

Monique Tie − *Department of Chemistry, University of Toronto, Toronto, Ontario M5S 3H6, Canada*

https://doi.org/10.1021/acs.nanolett.2c04918
Nano Lett. XXXX, XXX, XXX−XXX

Sean Colford − *Department of Physics, University of Toronto, Toronto, Ontario M5S 3H6, Canada*
Marek Niewczas − *Department of Materials Science and Engineering, McMaster University, Hamilton, Ontario L8S 4L7, Canada;* orcid.org/0000-0002-8529-7194
Ryan Baumbach − *National High Magnetic Field Laboratory, Tallahassee, Florida 32310, United States*

Complete contact information is available at: https://pubs.acs.org/10.1021/acs.nanolett.2c04918

Author Contributions

[⊥]M.T. and S.C. contributed equally to this work.

Notes

The authors declare no competing financial interest.

■ ACKNOWLEDGMENTS

This work was supported by the Natural Science and Engineering Research Council for Canada. Additionally, this work made use of a Quantum Design MPMS-3 supported by NSF (DMR-1920086) and the Cornell Center for Materials Research Shared Facilities which are supported through the NSF MRSEC program (DMR-1719875). A portion of this work was performed at the National High Magnetic Field Laboratory, which is supported by the National Science Foundation Cooperative Agreement No. DMR-1644779 and the State of Florida.

■ REFERENCES

(1) Wirth, S.; Steglich, F. Exploring heavy fermions from macroscopic to microscopic length scales. *Nature Reviews Materials* **2016**, *1*, 16066.
(2) Imada, M.; Fujimori, A.; Tokura, Y. Metal-insulator transitions. *Rev. Mod. Phys.* **1998**, *70*, 1039−1263.
(3) Georges, A.; Kotliar, G.; Krauth, W.; Rozenberg, M. J. Dynamical mean-field theory of strongly correlated fermion systems and the limit of infinite dimensions. *Rev. Mod. Phys.* **1996**, *68*, 13−125.
(4) Basov, D. N.; Averitt, R. D.; van der Marel, D.; Dressel, M.; Haule, K. Electrodynamics of correlated electron materials. *Rev. Mod. Phys.* **2011**, *83*, 471−541.
(5) Lee, P. A.; Nagaosa, N.; Wen, X.-G. Doping a Mott insulator: Physics of high-temperature superconductivity. *Rev. Mod. Phys.* **2006**, *78*, 17−85.
(6) Kondo, J. Resistance minimum in dilute magnetic alloys. *Prog. Theor. Phys.* **1964**, *32*, 37−49.
(7) Sarachik, M.; Corenzwit, E.; Longinotti, L. Resistivity of Mo-Nb and Mo-Re alloys containing 1% Fe. *Phys. Rev.* **1964**, *135*, A1041−A1045.
(8) Gang, T.; Yilmaz, M. D.; Ataç, D.; Bose, S. K.; Strambini, E.; Velders, A. H.; de Jong, M. P.; Huskens, J.; van der Wiel, W. G. Tunable doping of a metal with molecular spins. *Nat. Nanotechnol.* **2012**, *7*, 232.
(9) Liang, W.; Shores, M. P.; Bockrath, M.; Long, J. R.; Park, H. Kondo resonance in a single-molecule transistor. *Nature* **2002**, *417*, 725.
(10) Park, J.; Pasupathy, A. N.; Goldsmith, J. I.; Chang, C.; Yaish, Y.; Petta, J. R.; Rinkoski, M.; Sethna, J. P.; Abruña, H. D.; McEuen, P. L.; Ralph, D. C. Coulomb blockade and the Kondo effect in single-atom transistors. *Nature* **2002**, *417*, 722.
(11) Zhang, Y.-H.; Kahle, S.; Herden, T.; Stroh, C.; Mayor, M.; Schlickum, U.; Ternes, M.; Wahl, P.; Kern, K. Temperature and magnetic field dependence of a Kondo system in the weak coupling regime. *Nat. Commun.* **2013**, *4*, 2110.
(12) Parks, J. J.; Champagne, A. R.; Hutchison, G. R.; Flores-Torres, S.; Abruña, H. D.; Ralph, D. C. Tuning the Kondo effect with a mechanically controllable break junction. *Phys. Rev. Lett.* **2007**, *99*, 026601.
(13) Yu, L. H.; Natelson, D. The Kondo effect in C_{60} single-molecule transistors. *Nano Lett.* **2004**, *4*, 79−83.
(14) Atxabal, A.; Ribeiro, M.; Parui, S.; Urreta, L.; Sagasta, E.; Sun, X.; Llopis, R.; Casanova, F.; Hueso, L. E. Spin doping using transition metal phthalocyanine molecules. *Nat. Commun.* **2016**, *7*, 13751.
(15) Goldhaber-Gordon, D.; Shtrikman, H.; Mahalu, D.; Abusch-Magder, D.; Meirav, U.; Kastner, M. A. Kondo effect in a single-electron transistor. *Nature* **1998**, *391*, 156−159.
(16) Grobis, M.; Rau, I. G.; Potok, R. M.; Goldhaber-Gordon, D. In *Handbook of Magnetism and Advanced Magnetic Materials*; Kronmüller, H., Parkin, S., Eds.; Wiley: New York, 2007.
(17) Dutta, P.; Pal, S.; Seehra, M. S.; Anand, M.; Roberts, C. B. Magnetism in dodecanethiol-capped gold nanoparticles: Role of size and capping agent. *Appl. Phys. Lett.* **2007**, *90*, 213102.
(18) Crespo, P.; Litrán, R.; Rojas, T. C.; Multigner, M.; de la Fuente, J. M.; Sánchez-López, J. C.; García, M. A.; Hernando, A.; Penadés, S.; Fernández, A. Permanent Magnetism, Magnetic Anisotropy, and Hysteresis of Thiol-Capped Gold Nanoparticles. *Phys. Rev. Lett.* **2004**, *93*, 087204.
(19) Garitaonandia, J. S.; Insausti, M.; Goikolea, E.; Suzuki, M.; Cashion, J. D.; Kawamura, N.; Ohsawa, H.; Gil de Muro, I.; Suzuki, K.; Plazaola, F.; Rojo, T. Chemically induced permanent magnetism in Au, Ag, and Cu nanoparticles: Localization of the magnetism by element selective techniques. *Nano Lett.* **2008**, *8*, 661−667.
(20) Nealon, G. L.; Donnio, B.; Greget, R.; Kappler, J.-P.; Terazzi, E.; Gallani, J.-L. Magnetism in gold nanoparticles. *Nanoscale* **2012**, *4*, 5244−5258.
(21) Guerrero, E.; Muñoz-Márquez, M. A.; García, M. A.; Crespo, P.; Fernández-Pinel, E.; Hernando, A.; Fernández, A. Surface plasmon resonance and magnetism of thiol-capped gold nanoparticles. *Nanotechnology* **2008**, *19*, 175701.
(22) Guerrero, E.; Muñoz-Márquez, M. A.; Fernández-Pinel, E.; Crespo, P.; Hernando, A.; Fernández, A. Electronic structure, magnetic properties, and microstructural analysis of thiol-functionalized Au nanoparticles: role of chemical and structural parameters in the ferromagnetic behaviour. *J. Nanopart. Res.* **2008**, *10*, 179−192.
(23) Ramallo-López, J. M.; Giovanetti, L. J.; Requejo, F. G.; Isaacs, S. R.; Shon, Y. S.; Salmeron, M. Molecular conformation changes in alkylthiol ligands as a function of size in gold nanoparticles: X-ray absorption studies. *Phys. Rev. B* **2006**, *74*, 073410.
(24) Tie, M.; Dhirani, A.-A. Conductance of molecularly linked gold nanoparticle films across an insulator-to-metal transition: From hopping to strong Coulomb electron-electron interactions and correlations. *Phys. Rev. B* **2015**, *91*, 155131.
(25) Tie, M.; Gravelsins, S.; Niewczas, M.; Dhirani, A.-A. Large Kondo effect in assemblies of Au nanoparticles linked with alkanedithiol electron bridges. *Nanoscale* **2019**, *11*, 5395−5401.
(26) Liao, J.; Blok, S.; van der Molen, S. J.; Diefenbach, S.; Holleitner, A. W.; Schönenberger, C.; Vladyka, A.; Calame, M. Ordered nanoparticle arrays interconnected by molecular linkers: electronic and optoelectronic properties. *Chem. Soc. Rev.* **2015**, *44*, 999−1014.
(27) Liao, J.; Bernard, L.; Langer, M.; Schönenberger, C.; Calame, M. Reversible formation of molecular junctions in 2D nanoparticle arrays. *Adv. Mater.* **2006**, *18*, 2444−2447.
(28) Hori, H.; Yamamoto, Y.; Iwamoto, T.; Miura, T.; Teranishi, T.; Miyake, M. Diameter dependence of ferromagnetic spin moment in Au nanocrystals. *Phys. Rev. B* **2004**, *69*, 174411.
(29) Cronenwett, S. M.; Oosterkamp, T. H.; Kouwenhoven, L. P. A tunable Kondo effect in quantum dots. *Science* **1998**, *281*, 540−544.
(30) Nagaoka, K.; Jamneala, T.; Grobis, M.; Crommie, M. Temperature dependence of a single Kondo impurity. *Phys. Rev. Lett.* **2002**, *88*, 077205.
(31) Frota, H. O. Shape of the Kondo resonance. *Phys. Rev. B: Condens. Matter Mater. Phys.* **1992**, *45* (3), 1096−1099.
(32) Moshe, A.; Bachar, N.; Lerer, S.; Lereah, Y.; Deutscher, G. Multi-Level Kondo effect and enhanced critical temperature in

nanoscale granular Al. *Journal of Superconductivity and Novel Magnetism* **2018**, *31*, 733−736.
(33) Florens, S.; San José, P.; Guinea, F.; Georges, A. Coherence and Coulomb blockade in single-electron devices: A unified treatment of interaction effects. *Phys. Rev. B* **2003**, *68*, 245311.
(34) Wu, L.; Nikitin, S. E.; Brando, M.; Vasylechko, L.; Ehlers, G.; Frontzek, M.; Savici, A. T.; Sala, G.; Christianson, A. D.; Lumsden, M. D.; et al. Antiferromagnetic ordering and dipolar interactions of $YbAlO_3$. *Phys. Rev. B* **2019**, *99*, 195117.
(35) Coleman, P. Heavy Fermions: Electrons at the edge of magnetism. In *Handbook of Magnetism and Advanced Magnetic Materials*; John Wiley & Sons, Ltd., 2007; Vol. *38*, pp 1−54.
(36) Hernando, A.; Crespo, P.; García, M. A.; Coey, M.; Ayuela, A.; Echenique, P. M. Revisiting magnetism of capped Au and ZnO nanoparticles: Surface band structure and atomic orbital with giant magnetic moment. *physica status solidi (b)* **2011**, *248*, 2352−2360.
(37) Hanna, A.; Tinkham, M. Variation of the Coulomb staircase in a two-junction system by fractional electron charge. *Phys. Rev. B* **1991**, *44*, 5919−5922.
(38) Süllow, S.; Aronson, M.; Rainford, B.; Haen, P. Doniach phase diagram, revisited: From ferromagnet to Fermi liquid in pressurized $CeRu_2Ge_2$. *Phys. Rev. Lett.* **1999**, *82*, 2963−2966.

https://doi.org/10.1021/acs.nanolett.2c04918
Nano Lett. XXXX, XXX, XXX−XXX